2024 Paris Session

10667
B4: DC systems and power electronics
PS2: FACTS and power electronics

Experimental validation of the General Power Theory using Power Hardware-in-the-Loop - Opportunities for New Converter Controls

Pitambar JANKEE* **C. Trevor GAUNT** **Zhiwang FENG** **Graeme BURT**
University of Cape Town, South Africa
jnkpit001@myuct.ac.za ct.gaunt@uct.ac.za
University of Strathclyde, United Kingdom
zhiwang.feng@strath.ac.uk graeme.burt@strath.ac.uk

SUMMARY

Concept models, theories, and definitions of electric power quantities feed into the control of power-electronic converters and compensators. A definition of power quantities based on a measurement model respecting the laws of physics of circuits is therefore important for the optimal control of the energy injected into the grid from power-electronic converters.

Most power definitions use reactive power (Q) as a parameter defined in the average domain. However, Q is always zero if calculated as an average value within a fundamental frequency cycle. The physical interpretation of Q, especially during conditions of unbalance and harmonic distortion, is unclear.

The General Power Theory (GPT) for electrical circuits provides a rigorous approach to identifying the reference currents to be drawn from or injected into the system by a compensator or inverter to minimise power delivery loss and improve relative power delivery efficiency. It can be applied even in conditions of unbalance and harmonic distortion. Electromagnetic Transient (EMT) simulations have shown that minimum loss can be achieved using GPT-control of power-electronic converters instead of conventional approaches. This paper focuses on the application of the novel theory to power electronic converter control. It demonstrates through experimental validation the feasibility of a fundamentally new approach to converter control that may prove invaluable as the challenges of inverter-dominated grids and grid forming converter coordination emerge.

The effect of applying *pq*-compensation and GPT-compensation in a 3-phase 4-wire test network with a source, delivery system and load was studied using Simulink-simulations. The EMT simulation results were validated with Controller Hardware-in-the-Loop (CHIL) tests using a Digital Real-Time Simulator (DRTS) from Typhoon HIL. In a collaboration between the Universities of Cape Town and Strathclyde under the ERIGrid 2.0 transnational access programme, the approach was tested practically using the Power Hardware-in-the-Loop (PHIL) approach on a DRTS test bed interfaced with a 10 kW converter retrofitted with GPT control.

The paper describes how the GPT's *abc* reference frame approach to compensator and inverter control can completely replace the use of power components defined in a fictitious rotating reference frame. Implications for the design of converters with harmonic and unbalance capabilities, and some relevant aspects of PHIL testing are also described.

Results from this study showed that compensation for a resistive and inductive load was achieved without the need for the concept of Q. The efficiency of power transfer to the load was improved, and the delivery losses decreased. It was also shown that a GPT-compensated system was more efficient than a *pq*-compensated system. The experience with testing and analysing electrical circuits using the GPT approach has shown that power systems' electromagnetic phenomena can be explained – and the system performance can be controlled and improved – simply using voltages and currents.

The consistency between the simulated and physical demonstration of the technology in a power system confirms the validity and usefulness of the GPT in measurement and control. It brings a novel concept to the field of power electronics and has implications for the standardisation of measurement devices and the control of power electronic hardware.

KEYWORDS

Control, Controller Hardware-in-the-Loop, Efficiency, Loss reduction, Power-electronic converter, Power Hardware-in-the-Loop, Testing

1. INTRODUCTION

The discussion of power terms, apparent power, and reactive power is not new to Cigre Sessions. One of Cigre's first study committees was "Power factor improvement" (Amélioration du facteur de puissance), which attracted regular Session papers on power factor correction and related topics. In a 1927 Session paper, Budeanu supplemented the vector power triangle of power P, reactive power Q, and apparent power S, with a second non-active component of distortion power. Following this paper, a survey (The Roumanian Questionnaire [1]) of all member countries was carried out for what became the "reactive power" committee. An alternative approach to power analysis proposed by Fryze in 1932 was discussed at the Cigre meetings in 1933, and strongly rejected by Budeanu and other members. For 60 years, Budeanu's approach was widely adopted in national and international standards and engineering science, although it was difficult to interpret the equations in terms of physical energy flow.

Decades after the early works, reacting to the emerging power electronic control of loads and converters, researchers identified the weaknesses of the theories of both Budeanu and Fryze [2, 3]. However, another fundamental weakness was embedded in both theories and most of those proposed by Czarnecki, Akagi, Depenbrock, Tenti, and others analysed a load supplied by an ideal voltage source, without considering the influence of the delivery system.

Interested in the physical performance of power systems, Malengret and Gaunt developed a new power theory [4 - 6]. This theory applies generally for any number of delivery wires, unbalance, and distortion, and with a load, source, or another network at the point of connection (PoC). Like Budeanu's theory, the power components are decomposed by frequency, but power is not a vector quantity. As in Fryze's theory, a current has two components, one delivering power and a second that incurs loss without delivering power, although it turned out that these components are not orthogonal. Named for its generality, the novel General Power Theory (GPT) has applications in metering and control. Power electronic converters can be given reference currents in the *abc* frame to minimise the delivery loss associated with the power P_{PoC}.

The testing of the theory applied to control has two main components:

- To confirm that a converter operating under GPT control can produce the currents needed for optimum delivery efficiency during stable operation.
- To show that the converter-controlled currents reduce the delivery loss beyond the level achieved by other power factor compensation approaches.

This paper describes the experimental validation of the GPT using CHIL and PHIL, and the opportunities this presents for new converter controls.

Section 2 provides only a brief outline of the theory because the details have already been published. Section 3 describes the approach to applying the theory to control practical 3-phase 3- and 4-wire converters. Section 4 describes a series of tests carried out on two different converters, focusing on the CHIL and PHIL tests and the results, which are discussed briefly. The paper concludes with some observations about the significance of the tests for new converter controls and relevant standards.

2. BASICS OF THE GENERAL POWER THEORY

The details of the derivation and proof of the GPT in linear algebra, and the equations for all the measurement terms and formulae in a spreadsheet are published in other papers [4, 5]. This section outlines briefly the GPT calculation process.

In any system with M wires, the wire voltages can be measured from any common reference, and the currents can be measured in only M-1 wires, because Kirchhoff's current law gives the current in the M^{th} wire. By Fourier's theorem of decomposition, samples of periodic distorted waveforms of voltages and currents can be separated by a Discrete Fourier Transform (DFT) into harmonic components of the fundamental frequency. Using the complex root mean square (crms) values of each component, any M-

wire system can be separated by frequency into H+1 sub-systems of AC and DC frequencies where H denotes the highest harmonic order.

The voltages and currents at the same frequency deliver power, but voltages and currents of different frequencies are orthogonal, and their product is zero power. The power delivered by each frequency sub-system is a scalar quantity. By the principle of superposition, the total power delivered by the system is the algebraic sum of the power of each of the H+1 sub-systems.

Based on the Helmholtz-Thévenin equivalent impedance theorem, the impedance of each wire between an equivalent source (Thévenin point) and the PoC at each frequency can be measured from the PoC by one of the many published passive or active techniques [7, 8]. By Ohm's law, the current and impedance give the voltage across the equivalent impedance. The voltage of the equivalent ideal source of each wire can be calculated using Kirchhoff's voltage law.

These principles are illustrated in Figure 1, which shows one of the subsystems.

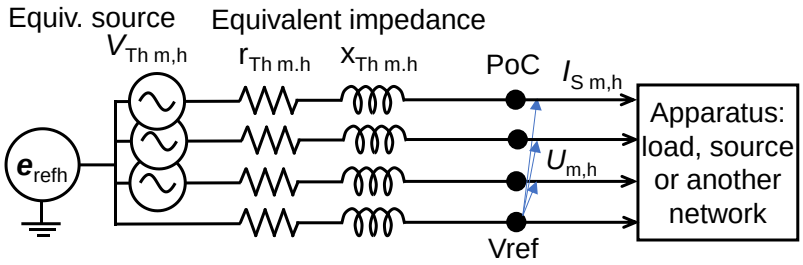

Figure 1: A subsystem defined by its harmonic order, showing an apparatus in the context of the equivalent 3-phase, 4-wire delivery system to which is connected at the PoC.

By weighting the voltage and current vectors at the Thévenin point with the resistance array of the delivery network, a quadratic equation can be set up using the law of conservation of energy:

$$||\boldsymbol{I}_A'||^2 - ||\boldsymbol{V}_{Th(null)}'||\ ||\boldsymbol{I}_A'|| + P_{PoC} = 0 \qquad (1)$$

where: $||\boldsymbol{I}_A'||^2$ is the minimum loss due to the resistance-weighted active (optimal) current $||\boldsymbol{I}_A'||$,
$||\boldsymbol{V}_{Th(null)}'||$ is the resistance weighted voltage at the Thévenin point,
$||\boldsymbol{V}_{Th(null)}'||\ ||\boldsymbol{I}_A'||$ is the optimum power P_{ThOpt} at the Thévenin point,
P_{PoC} is the power measured at the PoC, which treats the load as a constant power model, and
$'$ denotes resistance weighting.

The solution of the quadratic equation leads to the optimum active current component $\boldsymbol{I}_A$.

The conventional form of apparent power as the maximum power that could be delivered with the same voltages and currents aligned, and therefore the same original loss, but as defined at the source instead of the PoC for maximum efficiency, is:

$$AP_{SYS} = ||\boldsymbol{V}_{Th(null)}'||\ ||\boldsymbol{I}_S'|| \qquad (2)$$

This leads to a physically interpretable dimensionless index of relative power delivery efficiency. The power factor PF_{SYS} is given by the square root of the ratio of the minimum (or optimal) delivery loss $||\boldsymbol{I}_A'||^2$ to the actual delivery loss $||\boldsymbol{I}_S'||^2$ or as:

$$PF_{SYS} = ||\boldsymbol{I}_A'|| \ / \ ||\boldsymbol{I}_S'|| = P_{ThOpt} \ / \ AP_{SYS} \qquad (3)$$

Thus, the complete set of power terms associated with the apparatus at the PoC is P_{PoC}, the actual and optimum loss, and the system's apparent power, all measured in Watts. PF_{SYS} is an index of performance and $PF_{SYS} = 1$ occurs when current components are aligned with voltage components at the Thévenin point – not at the PoC.

The measurement model is extended for application to control by calculating a proportionality factor K_A that distributes the optimal power at the Thévenin point in proportion to the voltages and inversely to the wire resistances:

$$K_A = P_{ThOpt} / \|\boldsymbol{V}_{Th(null)}'\|^2 \quad (4)$$

The optimally distributed current components, which can be controlled by a converter at the PoC are:

$$I_{A\,m,h} = K_A\, V_{Th\,m,h(null)}/r_{m,h} \quad (5)$$

Knowing the optimum current $\boldsymbol{I}_A$ gives the currents to be injected or withdrawn by a shunt compensator. The converter currents are not orthogonal to the active current. The compensation current is not the same current as in the operational definition of reactive power as a component orthogonal to power.

The same equations apply to an inverter injecting power into the delivery system. The optimum injection currents are the active currents that incur the minimum delivery loss.

3. IMPLEMENTING THE CONVERTER CONTROL

Converter control involves measurement of the voltages and currents at the PoC, signal conditioning, digital signal processing, calculation of the setpoint currents using specific power theories and control of these currents using suitable linear or non-linear techniques. The response of the power system depends on the injected converter currents. Therefore, applying a valid and representative power theory to calculate the setpoint currents for the converter is important to optimise the efficiency of power delivery.

Figure 2 shows the calculation of the setpoint currents for a converter controlled by the *pq*-theory. The *pq*-theory is a time-domain instantaneous control approach. It uses Clarke's transform to convert voltages and currents from the *abc* reference frame to the $\alpha\beta0$ reference frame. Using the $\alpha\beta0$ quantities, three power components are calculated: instantaneous active power ($p_{\alpha\beta}$), instantaneous zero sequence active power (p_0), and instantaneous imaginary power ($q_{\alpha\beta}$). $p_{\alpha\beta}$ and $q_{\alpha\beta}$ may be decomposed by frequency into DC quantities ($\overline{p_{\alpha\beta}}$, $\overline{q_{\alpha\beta}}$) and AC quantities ($\widetilde{p_{\alpha\beta}}$, $\widetilde{q_{\alpha\beta}}$,) using digital filters. Depending on the role of the converter, setpoint currents are calculated from the power components and the voltages. In compensator mode of operation, the setpoint currents are calculated from p_0, $\widetilde{p_{\alpha\beta}}$ and $q_{\alpha\beta}$. In inverter mode for which present standards require unity power factor injection, only $p_{\alpha\beta}$ is required to generate the setpoint currents as $\alpha\beta0$ quantities. Control can be achieved either in the $\alpha\beta0$ reference frame or in the *abc* reference frame after applying an inverse Clarke transform to the $\alpha\beta0$ currents [9].

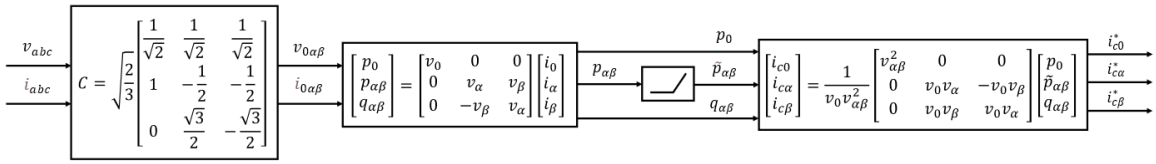

Figure 2: Setpoint current generation using the *pq*-theory.

Figure 3 shows the calculation of setpoint currents based on the GPT. This is fundamentally different from the *pq*-theory approach where the aim is to align the voltages and currents at the PoC. The GPT setpoint currents for a converter are calculated by subtracting the measured PoC currents from their optimal values $I_{A\,m,h}$.

Control using the GPT does not make use of reactive power since orthogonal power components cannot lead to optimised system performance. The setpoint currents generated in the *abc* reference frame avoid computational delays caused by reference frame transformation such as the Clarke transform adopted by the *pq*-theory.

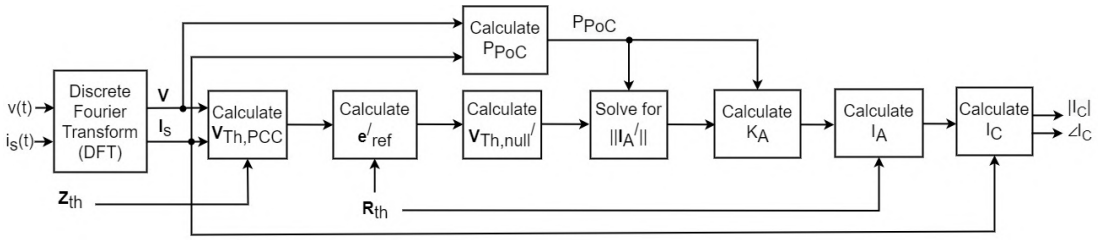

Figure 3: Setpoint current generation using the GPT.

Because of the inherent link between the reference frame currents and the frequency and voltage of the system, designing controllers based on reference frame transformation is straightforward. A GPT-controlled converter can provide both frequency and voltage support. Frequency support may be achieved by regulating the optimal power injected into the grid using additional control loops and by controlling the phase angle (using a Phase Locked Loop - PLL) between the grid voltage and the converter voltage. Moreover, since the GPT determines the PoC voltage change when the converter injects the optimal currents, droop control can be used for voltage support. Since the *pq*-theory and the GPT determine sinusoidal setpoint currents, current control using Proportional Resonant (PR) controllers are recommended as they provide high gain at the control frequencies and good tracking performance with minimal steady-state errors. Both the *pq*- and GPT control approaches require one PR controller for each phase. To track multiple frequency components, multi-resonant PR controllers with delay compensation for higher-order harmonics are necessary.

Contrary to present industry standards such as the IEEE 519 [10], the GPT emphasises that minimum power delivery loss can only be achieved when harmonic power is controlled. Therefore, a GPT-controlled converter's output filter should not attenuate harmonic currents being drawn or injected. In the case of LCL filters, mostly applied in converter systems, proper placement of the resonant frequency during design is essential to avoid interference with the control bandwidth. Moreover, damping of the resonance effect using passive or active methods can be achieved using GPT control to ensure the stability of the control loop. Another important consideration is that the PLL coupled with a GPT-based converter should be able to track the grid voltages even when they are distorted and unbalanced.

4. TESTS AND RESULTS

In this section, testing of three different converters with the novel control method in the *abc* reference frame is discussed. EMT and CHIL test results show and compare the effect of applying *pq*-compensation and GPT-compensation to systems with balanced resistive loads and balanced resistive-inductive loads. PHIL results using a physical GPT-controlled converter are followed by a brief discussion of the challenges faced with tests in an industry-scale network.

4.1 Preliminary functional tests on 20 kW 3p4w converter

It was necessary to verify whether control in the *abc* reference frame was achievable. Such an approach has not been found in the literature except for hysteresis-based methods in which varying switching frequencies introduce complexities in the filter design. As shown in Figure 4, a 20 kW 3-phase 4-wire (3p4w) Neutral Point Clamped (NPC) converter coupled with a passively damped LCL filter was designed and built at the University of Cape Town (UCT). Using model-based design in Simulink, a control algorithm in the *abc* reference frame with fundamental frequency PR controllers was developed. Synchronisation to the grid voltage was achieved using a single-phase PLL. The C-code for the control process was deployed on a Texas Instrument F28069M LaunchPad using automatic code generation.

The dc-bus voltage was slowly increased to 700 V and a ramp was applied to the setpoint current of 15 Arms. The voltage and current measured on phase A are shown in Figure 4. The THD in voltage was 2.65 % and 3.63 % in current. The distortion can be reduced by adding harmonic regulators in parallel to the fundamental frequency PR controller.

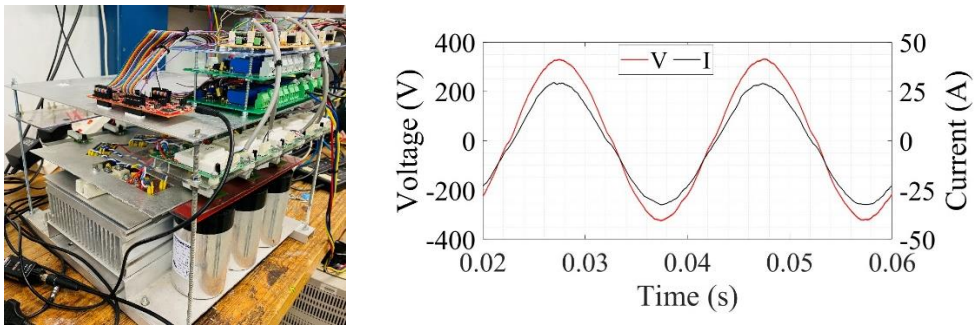

Figure 4: 20 kW 3-phase 4-wire NPC converter designed and built at UCT and the test results.

In these preliminary tests, we assumed that the grid frequency was 50 Hz. The PR controller did not adapt to the actual grid frequency and introduced steady-state errors in the controller response. The tests showed that the PR controller needed a frequency input to update the resonant control frequency at every sampling interval, with high gain at exactly the grid frequency (and its multiples).

4.2 Preliminary Comparison of EMT Simulation and CHIL with Balanced Resistive Load

Having experimentally verified, using the 20 kW converter, that control in the *abc* reference frame was achievable, we were lent a commercial 80 kW 3-phase 3-wire Active NPC (ANPC) converter. The commercial converter has the advantages of industry-compliant measurement systems, stable 3-phase PLL for grid synchronisation, advanced phase-shifted PWM and safety controls. Therefore, it was only required to convert the existing dq0-based current control algorithm to the GPT's *abc*-reference frame control. From our experience gained with the 20 kW converter, we added 5th and 7th harmonic regulators in parallel to the fundamental frequency PR controller to reduce the harmonic distortion in the converter outputs. Moreover, a frequency-adaptive PR controller was used by feeding the frequency signal from the PLL to the PR controller. A third addition was the introduction of active damping using capacitor-current feedback to attenuate the resonance effect of the LCL filter. The converter specifications, retrofitting process, implementation steps and experimental testing of the novel control technique applied to the 80 kW converter were presented at a CIGRE Regional Conference [11].

Models of the 80 kW GPT-controlled converter and a power system with a balanced resistive load shown in Figure 5 were developed in Simulink and Schematic Editor of Typhoon HIL. The effect of applying *pq*-theory compensation and GPT-compensation to the practical power system model were compared using both EMT simulations and CHIL tests. The CHIL tests used a Typhoon 402 DRTS and an external Texas Instrument F28335 microcontroller. In Simulink which is an EMT software, to understand the effectiveness of compensation using the converter, injection of the compensating currents at the PoC was made both using an ideal controlled current source (CCS) and the full model of the converter (Conv).

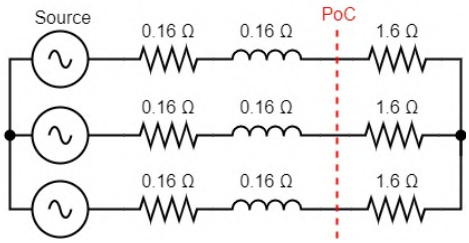

Figure 5: 3-phase 3-wire test circuit. The ideal source was initialised to V_{ab} = 441.814∠35.194°.

Figure 6 presents the CHIL test results showing the PoC voltages and source currents before and during GPT compensation and the converter output currents. With a model of the converter used to inject the compensating currents, the PoC voltages were distorted due to the switching frequency current harmonics introduced by the converter. Injection using an ideal current source in Simulink showed no voltage distortion. With an ideal current source, the reference compensating currents, and injected currents were perfectly matched. There was no distortion of the currents since the injection was "ideal".

Practically, any compensation for a resistive load requires small compensating currents relative to the rated current of the converter. This means that the modulation index is small and distortion is significant. The converter operates in an "idling mode". At higher compensating currents and with the same set of controller parameters, the distortion is reduced, for example when compensating for a resistive-inductive load.

Table I summarises the power at the PoC, power loss, conventional power factor, and GPT-defined system power factor before compensating currents are injected. The same power components are shown in Table II for the condition when compensating currents are injected using the GPT. The *pq*-theory calculates zero compensating currents for such a test system. The results obtained from the EMT simulation and the CHIL tests are effectively the same. Small differences arise due to the software components which may have been modelled differently in both software, latency introduced in input and output (IO) interfaces, or inefficiencies such as computational delays when the control algorithm runs on a microcontroller.

The GPT-controlled compensation reduced the losses below those of the uncompensated system. Conventionally, the load would be a unity power factor load. The GPT determines that the power factor before compensation was 0.9950 and it is possible to reduce the loss by injecting balanced fundamental frequency active currents. GPT compensation improved the system power factor while the conventional power factor dropped. The *pq*-compensation does not compensate for such a load because it fails to identify the active current components which incur minimum loss.

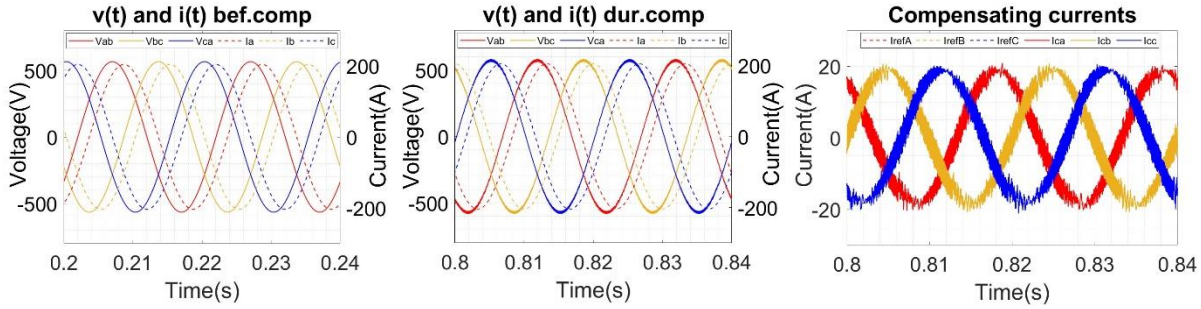

Figure 6: 3-phase 3-wire CHIL test results showing PoC v(t) and i(t) before and during GPT compensation, and the compensating currents injected.

Table I: Power, power loss, and power factors before compensation

Power Quantities	***EMT***	***CHIL***
Power at PoC, P_{PoC}	100000.13	99999.34
Power loss, P_{LOSS}	10000.03 10.000 % P_{PoC}	9999.93 10.000 % P_{PoC}
Conventional power factor	1.0000	1.0000
GPT power factor, PF_{SYS}	0.9950	0.9950

Table II: Power, power loss, and power factors during GPT compensation

Power Quantities	***EMT - CCS***	***EMT - Conv***	***CHIL***
Power at PoC, P_{PoC}	100739.92	100749.83	100744.50
Power loss, P_{LOSS}	10064.39 9.990 % P_{PoC}	10066.14 9.991 % P_{PoC}	10068.73 9.994 % P_{PoC}
Conventional power factor	0.9960	0.9960	0.9960
GPT power factor, PF_{SYS}	1.0000	1.0000	1.0000

4.3 EMT Simulation and CHIL Test on 10 kW 3p4w Converter

Through the ERIGrid 2.0 transnational lab access programme, we arranged to test the 80 kW converter at the University of Strathclyde but problems with customs clearance delayed its delivery. The opportunity was given to retrofit a 10 kW 3-phase 4-wire converter already available at the Dynamic Power System Laboratory (DPSL). Given the prior experience on two converters, retrofitting of GPT

control on the 10 kW converter was carried out within 3 days. The converter specifications, implementation of GPT control with active damping using capacitor-current feedback, and retrofitting process on the 10 kW converter are explained in another paper [12].

To compare the effect of GPT- and *pq*-controlled compensation using the 10 kW converter model, two test models were developed in Simulink and Schematic Editor of Typhoon HIL. Figure 7 shows the base case test system designed with a 20 kW balanced resistive load, a delivery system which results in a power delivery loss of 10 % (2 kW) of the load power, and source voltage initialised such that the PoC voltage is 230 V. This test system (left) was called Test 1. It also shows (right) the same delivery system with a balanced 20 kW resistive-inductive load having an impedance factor of 0.85 for Test 2.

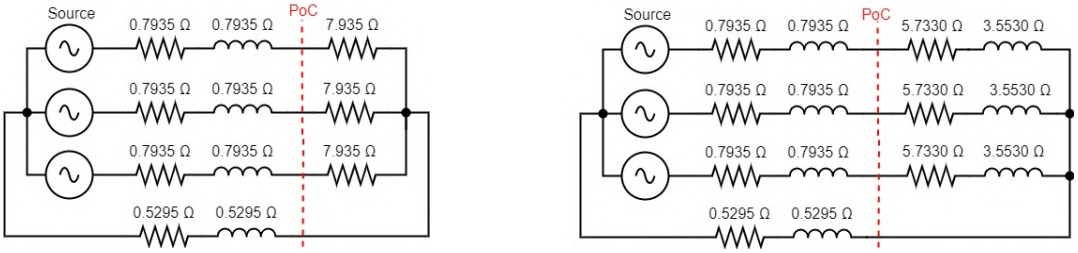

Figure 7: 3-phase 4-wire circuit with the ideal source initialised to V_{an} = 254.043∠5.194°.
Test 1 (left) with a resistive load. Test 2 (right) with R-L load.

Figure 8 shows the PoC voltages and currents measured before and during compensation from the CHIL test 1. The compensating currents injected using the converter model are also shown. Table III summarises the results of the EMT and CHIL tests. The results were closely matched with minor differences arising due to software and IO interfaces as explained in section 4.2. Before compensation, the PoC currents and voltages were in phase. During compensation, the currents in each wire were leading the corresponding wire voltages. The resulting effect appeared on the source side, where the voltages and currents were aligned. Both in EMT and CHIL, the results showed that the GPT compensated for a balanced resistive load and caused a decrease in the delivery losses. This is significantly different from all other conventional approaches to compensation such as the *pq*-theory which assume that the efficiency of power delivery is already optimised because the load is a resistor. The distortion of the compensating current by the "idling" converter is apparent.

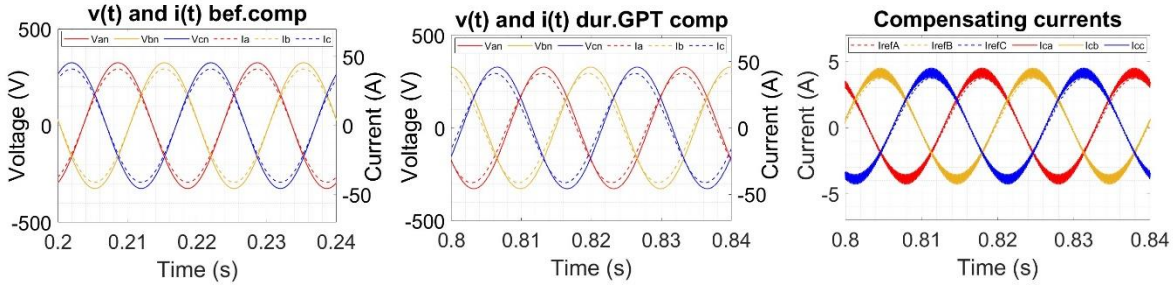

Figure 8: 3-phase 4-wire CHIL test 1 results showing PoC v(t) and i(t) before and during GPT compensation and the injected compensating currents.

Table III: Test 1 EMT and CHIL results

Power Quantities	***Before Compensation***		***During GPT Compensation***	
	EMT	***CHIL***	***EMT***	***CHIL***
Power at PoC, P_{PoC}	20000.13	19999.82	20147.75	20120.79
Power loss, P_{LOSS}	2000.03 10.000 % P_{PoC}	1999.98 10.000 % P_{PoC}	2013.60 9.994 % P_{PoC}	2008.78 9.984 % P_{PoC}
Conventional power factor	1.0000	1.0000	1.0000	1.0000
GPT power factor, PF_{SYS}	0.9950	0.9950	0.9960	0.9952

Figure 9 shows the results of CHIL test 2 before compensation and during compensation using the GPT and the *pq*-theory. Table IV summarises the results. A relatively good correlation between EMT

simulation and CHIL is evident. Compensation using both the GPT and the *pq*-theory reduced the phase shift between currents and the corresponding wire voltages. However, the losses decreased more using GPT compensation compared to *pq*-compensation. Both the conventional power factor for an apparatus and the GPT-defined power factor for the system improved with compensation. However, the GPT-compensated system was always more efficient in power delivery (indicated by PF_{SYS}) than the *pq*-compensated system. In terms of the controller response, steady-state errors between the reference currents and injected currents were negligible. The controller showed good tracking performance. Since the compensating currents injected were much higher than in test 1, there was negligible current and voltage distortion with the same set of controller parameters.

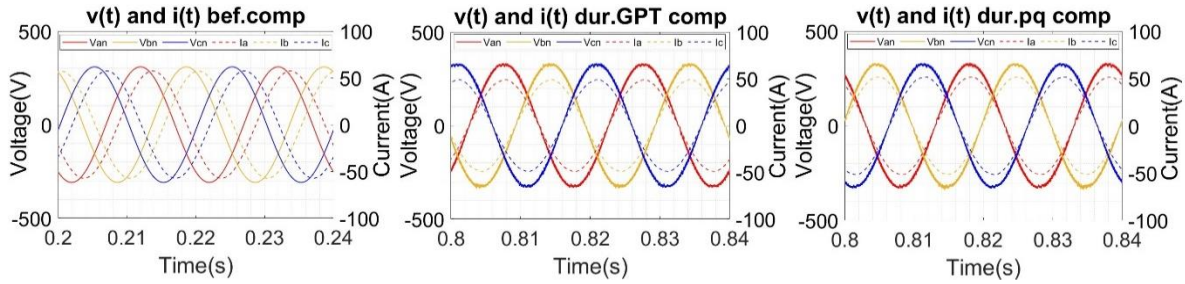

Figure 9: 3-phase 4-wire CHIL test 2 results showing PoC v(t) and i(t) before and during compensation using the GPT and *pq*-theory.

Table IV: Test 2 EMT and CHIL results

Power Quantities	***Before Compensation***		***During GPT Compensation***		***During pq Compensation***	
	EMT	***CHIL***	***EMT***	***CHIL***	***EMT***	***CHIL***
P_{PoC}	18052.38	18051.30	19247.75	19357.56	19564.27	20367.48
P_{LOSS}	2498.61 13.84 % P_{PoC}	2498.59 13.84 % P_{PoC}	1836.71 9.54 % P_{PoC}	1843.13 9.52 % P_{PoC}	1916.66 9.80 % P_{PoC}	2064.51 10.14 % P_{PoC}
conv pf	0.8500	0.8500	1.0000	1.0000	0.9996	0.9997
PF_{SYS}	0.7951	0.7951	0.9951	0.9957	0.9919	0.9921

4.4 PHIL tests with 10 kW compensator

PHIL simulations of tests 1 and 2 were carried out by injecting compensating currents using the physical 10 kW converter available at the DPSL. Figure 10 shows the PHIL test bed with the 10 kW converter, grid emulator or power amplifier and the DRTS. The power system models of test 1 and 2 were modelled in RSCAD software. They run in real-time on the DRTS. PoC voltages and currents were measured and exported in real-time to the 10 kW converter through the power amplifier. The 10 kW converter implements the GPT algorithm and sends (real) compensating currents back to the power system model in the simulation environment.

For test 1, since the compensating currents are relatively small compared to the rated converter current, the setpoint current for the converter was multiplied by a factor of 4. The real-time simulation interface allows a scaling of the current that feeds into the simulation model of the power network. Therefore, a factor of 0.25 was applied to rescale the converter output currents. Using this approach avoided the "idling mode" of the converter where high distortion due to the switching frequency harmonics would have otherwise been observed.

Figure 11 shows the PoC voltages, PoC currents and compensating currents from PHIL test 1. Table V summarises the results. Comparing Table III with Table V shows that the EMT simulation results, CHIL and PHIL test results were closely matched before and during GPT compensation. This validates the use of the three methods to test the effect on system performance by applying GPT compensation. The scaling of the reference compensating currents avoided the distortion caused by the "idling" mode of operation of the converter. The controller was effective in tracking the reference currents and operated stably in the PHIL test bed.

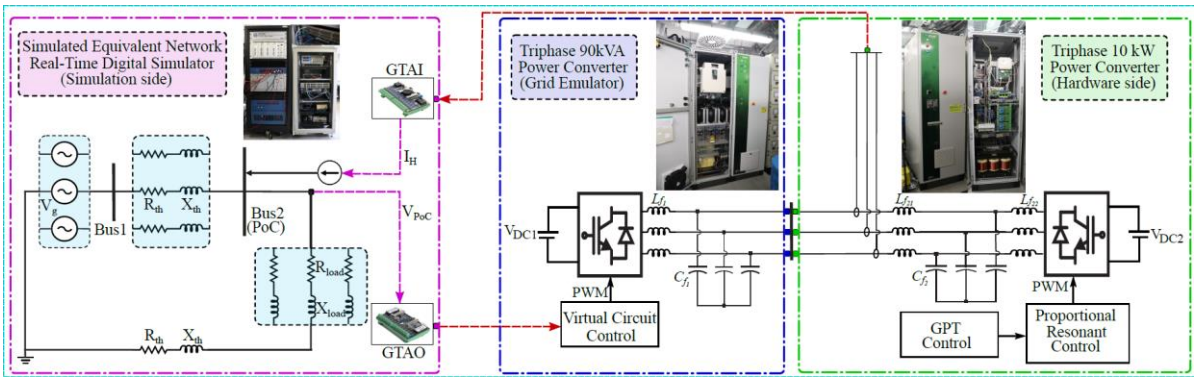

Figure 10: PHIL test bed showing the 10 kW converter, the power amplifier and an example of the real-time simulation model of the power network of test 2.

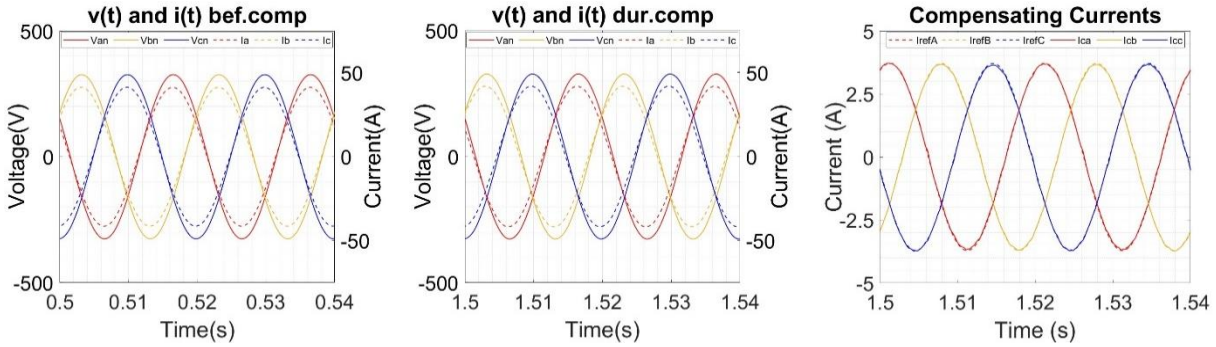

Figure 11: PHIL test 1 results showing PoC v(t) and i(t) before and during GPT compensation, and the compensating currents injected.

Table V: PHIL Test 1 results

Power Quantities	***Before Compensation***	***During GPT Compensation***
Power at PoC, P_{PoC}	20000.02	20152.52
Power loss, P_{LOSS}	2000.00 10.000 % P_{PoC}	2013.89 9.993 % P_{PoC}
Conventional power factor	1.0000	0.9960
GPT power factor, PF_{SYS}	0.9950	1.0000

Figure 12 presents the results of PHIL test 2 with the balanced resistive-inductive load and Table VI summarises the results. In this case, the PHIL results differed from the EMT and CHIL results. The differences can be explained by the fact that inductive components in the PHIL test bed caused problems during testing. Highly inductive circuits frequently tripped the converter and grid emulator. We suspected an instability within the PHIL test bed when the inductances of components were increased. Despite the differences, the effect of compensation on system performance was evident from the results. Without using the concept of reactive power, the GPT compensated for the avoidable loss in the system and improved the efficiency of power transfer to the load.

PHIL tests with distortion were not possible since we encountered difficulties interfacing the low-frequency component models with the high-frequency ones in RSCAD. We tried an alternative approach using controlled current sources to generate the distortion, but the software limitations could not be resolved. A PHIL test with unbalance will be presented in a subsequent paper.

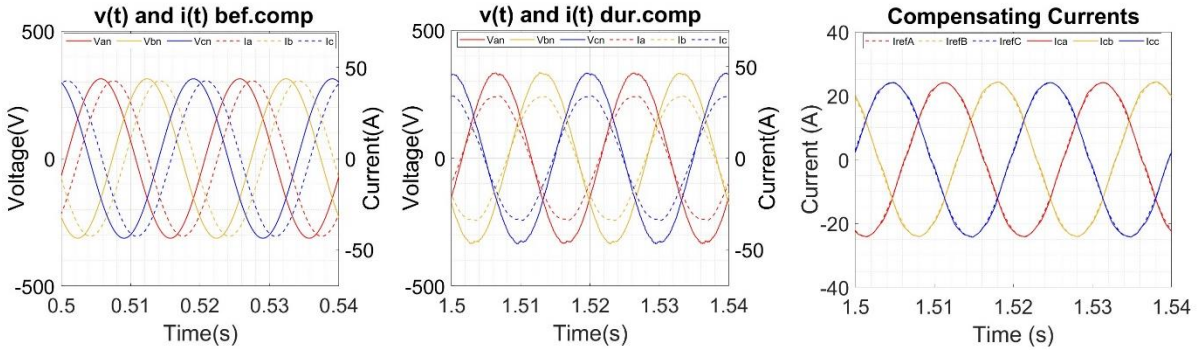

Figure 12: PHIL Test 2 results showing PoC v(t) and i(t) before and during GPT compensation, and the compensating currents injected.

Table VI: PHIL Test 2 results

Power Quantities	***Before Compensation***	***During GPT Compensation***
Power at PoC, P_{PoC}	16832.23	17019.47
Power loss, P_{LOSS}	2166.89 12.873 % P_{PoC}	1385.84 8.143 % P_{PoC}
Conventional power factor	0.8500	0.9984
GPT power factor, PF_{SYS}	0.7906	0.9997

4.5 PNDC tests with 80 kW converter

When the 80 kW converter discussed in section 4.2 arrived at the Power Network Demonstration Centre of the University of Strathclyde, testing of the application of GPT control started. Various problems arose and the tests could not be completed in the time available. The challenges faced and lessons learnt during experimental tests at PNDC are discussed in another paper [13].

5. CONCLUSION

The tests described in this paper achieved both the objectives set out in section 1 – a converter operating under GPT-control can produce the currents needed for optimum delivery efficiency, and these currents reduce the losses below the level achievable with *pq* control. The GPT-controlled converter responds appropriately to unbalance, distortion and the electrical environment represented by the equivalent delivery system impedance. Despite the suspected instability that arose in the PHIL testbed, the results of the EMT simulations, CHIL, and PHIL tests confirmed that the GPT-controlled compensation improved the efficiency of power delivery.

That distributed energy resources cannot be actively optimised as depicted in [14] is no longer a technical constraint. A new approach applying the GPT measurement model to controllers is especially appropriate for small systems and at the grid edge where distortion and unbalance occur, and in converter-dominated systems. However, the present grid codes based on conventional approaches to reactive power and power factor would need to be amended to require or at least allow different, more energy-efficient control.

ACKNOWLEDGEMENTS

We acknowledge the contribution to this research from the UCT Innovation Builder Fund, ERIGrid 2.0 (Grant No. 870620), Ario MeTaPower, University of Strathclyde for access to DPSL and PNDC, and Cape Peninsular University of Technology for access to TYPHOON HIL.

BIBLIOGRAPHY

[1] A.E. Knowlton, Reactive power concepts in need of clarification. Trans. AIEE, pp. 744-747, 1933.

[2] L.S. Czarnecki, Budeanu and Fryze: Two frameworks for interpreting power properties of circuits with nonsinusoidal voltages and currents. Electrical Engineering 80 (I997) 359-367.

[3] P.S. Filipski, Apparent power—a misleading quantity in the non-sinusoidal power theories: are all non-sinusoidal power theories doomed to fail? European Trans. Electrical Power, vol. 3, no 1, pp. 21–26, 1993. https://doi.org/10.1002/etep.4450030105.

[4] M. Malengret, C.T. Gaunt, Active currents, power factor, and apparent power for practical power delivery systems. IEEE Access, 2020. doi: 10.1109/ACCESS.2020.3010638.

[5] C.T. Gaunt, H.K. Chisepo, M. Malengret, Applying a physics-consistent general power theory to practical electricity systems with unbalance and periodic waveform distortion – Part 1: Implementation, testing, application to DG. Cigre Science and Engineering, Oct 2023. At https://cse.cigre.org/cse-n030.html.

[6] M. Malengret, C.T. Gaunt, inventors, University of Cape Town, proprietor: Frequency domain-based determination of currents for injection into a power network. UK Patent GB2582914, 29 Sep 2021.

[7] S. M. Abdelkader, D.J. Morrow, "Online Tracking of Thévenin Equivalent Parameters Using PMU Measurements," in IEEE Transactions on Power Systems, vol. 27, no. 2, pp. 975-983, May 2012, https://doi.org/10.1109/TPWRS.2011.2178868.

[8] A.V. Adebayo, C.T. Gaunt, K.O. Awodele, M. Malengret, Online Thévenin equivalent impedance measuring system. 2019 IEEE PES/IAS PowerAfrica, Abuja, Nigeria, 2019, pp. 295-300, https://doi.org/10.1109/PowerAfrica.2019.8928819.

[9] H. Akagi, Y. Kanazawa, K. Fujita, A. Nabae, Generalized theory of instantaneous reactive power and its application. Elect. Eng. Jpn., vol. 103, no. 4, pp. 58-66, 1983.

[10] IEEE Standard for Harmonic Control in Electric Power Systems, IEEE Standard 519, 2022.

[11] P. Jankee, L. Schmidt, C.T. Gaunt, M. Malengret, K. Litsoane, R. Yorke, Design, performance and testing of a converter under General Power Theory Control. CIGRE SA Regional Conference, Oct 2023.

[12] P. Jankee, C.T. Gaunt, M. Malengret, D. T. Oyedokun, Z. Feng, G. Burt, Revisiting the concept of reactive power for analysis and control of power system performance. (Unpublished.)

[13] P. Jankee, C.T. Gaunt, M. Malengret; I. Abdulhadi; B. Feizifar, et al., Challenges, solutions and lessons learnt from testing power system performance with a General Power Theory-controlled converter. 8th IEEE Workshop on the Electronic Grid (eGRID), Karlsruhe, Germany, 2023. https://doi.org/10.1109/eGrid58358.2023.10380824.

[14] B. Badrzadeh, Z. Emin, E. Hillberg, D. Jacobson, L. Kocewiak, et al., The need for enhanced power system modelling techniques and simulation tools. Cigre Science and Engineering, no. 017, pp. 30-46, 2020. At https://cse.cigre.org/cse-n017.html.